Contribution from Bell Laboratories,
Murray Hill, New Jersey 07974

Synthesis and Molecular and Electronic Structure of $[Ir(Se_4)((CH_3)_2PCH_2CH_2P(CH_3)_2)_2]Cl$, a Complex with a Five-Membered $IrSe_4$ Ring

A. P. GINSBERG,* J. H. OSBORNE,[1] and C. R. SPRINKLE

Received October 26, 1982

Square-planar $[Ir(dmpe)_2]Cl$ (dmpe = $(CH_3)_2PCH_2CH_2P(CH_3)_2$) reacts with Se_8 to form deep red $[Ir(Se_4)(dmpe)_2]Cl$, together with small amounts of deep purple $[Ir(Se_2)(dmpe)_2]Cl$. The purple compound contains side-on-bonded diselenium and is analogous to the known compounds $[Ir(Se_2)(dppe)_2]Cl$ (dppe = $(C_6H_5)_2PCH_2CH_2P(C_6H_5)_2$) and $[Rh(Se_2)(dmpe)_2]Cl$. Selenium abstraction with triphenylphosphine converts the Se_4 complex to the Se_2 complex. An X-ray structure determination on the Se_4 complex shows the crystals to be orthorhombic, space group *Fddd*, with a = 15.406 (5) Å, b = 26.792 (6) Å, c = 50.591 (13) Å, V = 20881.6 Å^3, and Z = 32. The cation has cis-octahedral geometry with the Se_4 group symmetrically chelated to the iridium at equatorial positions and each dmpe group chelating axial and equatorial positions. The $IrSe_4$ ring has a "half-chair" conformation, with the two central selenium atoms equidistant from, and on opposite sides of, the plane of the Ir atom and the two coordinated Se atoms. The mean Ir–Se (2.545 Å) and Se–Se (2.307 Å) distances are very similar to the values in $[Ir(Se_2)(dppe)_2]^+$. SCF–Xα–SW calculations on $[Ir(Se_4)(PH_3)_4]^+$ indicate that the Se_4 group in the complex is best described as an excited Se_4 molecule. Ir–Se_4 bonding is mainly via overlap of Ir $5d_{yz}$, $5d_{z^2}$ and $6p_x$ orbitals with Se 4p orbitals. pσ bonds form the main link between the Se atoms in the Se_4 group. In an EPA glass at liquid-nitrogen temperature, $[Ir(Se_4)(dmpe)_2]^+$ shows four absorption bands in the 300–700-nm region. These are assigned to one-electron transitions, with good agreement between the observed and calculated energies. The transitions are predominantly intra Se_4 ligand in character. The spin-allowed HOMO → LUMO transition corresponds to a shoulder at ~450 nm and is the lowest energy feature of the spectrum.

Introduction

Although a number of complexes are known in which an S_4 group chelates to a metal atom to form a five-membered ring,[2-8] the analogous chelation of an Se_4 group has been reported only in the compounds $(C_5H_5)_2MSe_4$ (M = Mo, W);[9] there has been no structural characterization of the MSe_4 ring. In this paper we report the preparation of the compound $[Ir(Se_4)(dmpe)_2]Cl$[10] by the reaction of *cyclo*-octaselenium with $[Ir(dmpe)_2]Cl$, a surprising result in view of the fact that only the diselenium adducts have been obtained from the reaction of Se_8 with $[Ir(dppe)_2]Cl$ and $[Rh(dmpe)_2]Cl$ and only the disulfur adducts from the reaction of S_8 with $[Ir(dmpe)_2]Cl$, $[Ir(dppe)_2]Cl$, and $[Rh(dmpe)_2]Cl$.[11] $[Ir(Se_4)(dmpe)_2]Cl$ may be converted to the side-on-bonded diselenium complex, $[Ir(Se_2)(dmpe)_2]Cl$, by selenium abstraction with triphenylphosphine. A single-crystal X-ray structure determination has shown that the $[Ir(Se_4)(dmpe)_2]^+$ cation contains an Se_4 group symmetrically chelated to the iridium atom to form a 5-membered ring with the "half-chair" conformation.[12] This is like the geometry of the MS_4 ring in $(\eta^5\text{-}C_5H_5)_2MS_4$ (M = Mo, W).[3,4] The Ir–Se and Se–Se distances are very similar to what is found in $[Ir(Se_2)(dppe)_2]^+$.[11]

In view of the current interest in the chemistry of complexes of di- and polychalcogenide groups[13] and the lack of information about electronic structure and bonding in these compounds,[14] we have studied the electronic spectrum of $[Ir(Se_4)(dmpe)_2]Cl$ and used the SCF–Xα–SW method to investigate the electronic structure of the model complex $[Ir(Se_4)(PH_3)_4]^+$. The Xα calculations lead us to conclude that the Se_4 group in $[Ir(Se_4)(PH_3)_4]^+$ is best described as an excited Se_4 molecule, just as the Se_2 group in $[Ir(Se_2)(PH_3)_4]^+$ is best thought of as a neutral molecule in an excited state.[14] Iridium is bound to the Se_4 group mainly by overlap of Ir $5d_{yz}$, $5d_{z^2}$, and $6p_x$ orbitals with Se 4p orbitals. The net Ir atom charge and electron configuration are essentially the same in $[Ir(Se_4)(PH_3)_4]^+$ as in $[Ir(Se_2)(PH_3)_4]^+$. In the Se_4 group, the selenium atoms are linked mainly by pσ bonds. Charge density maps indicate that the central Se–Se bond is stronger than the outer Se–Se bonds; this is in agreement with the observed Se–Se bond length alteration in the $IrSe_4$ ring.

The optical spectrum (300–700 nm) of $[Ir(Se_4)(dmpe)_2]Cl$ was measured in an EPA glass at liquid-nitrogen temperature. Four bands were observed and have been assigned to one-electron transitions; the observed band energies are in good agreement with the values calculated by the Xα transition-state method. All of the transitions are predominantly intra Se_4 ligand in character. A shoulder at ~450 nm is the lowest energy feature of the spectrum and corresponds to the spin-allowed HOMO → LUMO transition. The single largest

(1) 1981 summer research student at the Bell Laboratories. Present address: Department of Chemistry, University of Washington, Seattle WA.

(2) The following complexes containing chelating S_4 have been characterized crystallographically: $(\eta^5\text{-}C_5H_5)_2WS_4$,[3] $(\eta^5\text{-}C_5H_5)_2MoS_4$,[4] $[(S_4)_2MoS]^{2-}$,[5,6] $[(S_4)_2MoO]^{2-}$,[6] $[Mo_2S_{10}]^{2-}$,[6] $[Mo_2S_{12}]^{2-}$,[6] and NH_4CuS_4.[7] Some other S_4 complexes are mentioned in the literature survey in ref 8.

(3) Davis, B. R.; Bernal, I.; Köpf, H. *Angew. Chem., Int. Ed. Engl.* **1971**, *10*, 921–922. Davis, B. R.; Bernal, I. *J. Cryst. Mol. Struct.* **1972**, *2*, 135–142.

(4) Block, H. D.; Allman, R. *Cryst. Struct. Commun.* **1975**, *4*, 53–56.

(5) Simhon, E. D.; Baenziger, N. C.; Kanatzidis, M.; Draganjac, M.; Coucouvanis, D. *J. Am. Chem. Soc.* **1981**, *103*, 1218–1219.

(6) Draganjac, M.; Simhon, E.; Chan, L. T.; Kanatzidis, M.; Baenziger, N. C.; Coucouvanis, D. *Inorg. Chem.* **1982**, *21*, 3321–3332.

(7) Burschka, C. *Z. Naturforsch., B: Anorg. Chem., Org. Chem.* **1980**, *35B*, 1511–1513.

(8) Schmidt, M.; Hoffman, G. *Z. Naturforsch. B: Anorg. Chem., Org. Chem.* **1979**, *34B*, 451–455.

(9) Köpf, H.; Kahl, W.; Wirl, A. *Angew. Chem., Int. Ed. Engl.* **1970**, *9*, 801–802.

(10) The following abbreviations are used in this paper: dmpe, $(CH_3)_2PCH_2CH_2P(CH_3)_2$; dppe, $(C_6H_5)_2PCH_2CH_2P(C_6H_5)_2$; HOMO, highest occupied molecular orbital; LUMO, lowest unoccupied molecular orbital; EPA, 5:5:2 mixture of ethyl ether, isopentane, and ethyl alcohol.

(11) Ginsberg, A. P.; Lindsell, W. E.; Sprinkle, C. R.; West, K. W.; Cohen, R. L. *Inorg. Chem.* **1982**, *21*, 3666–3681.

(12) The "half-chair" and "envelope" conformations of MS_4 and MSe_4 rings are analogous to the conformations of cyclopentane with the same names.

(13) See, for example, ref 6 and 11 and the references cited therein and: Bolinger, C. M.; Rauchfuss, T. B.; Wilson, S. R. *J. Am. Chem. Soc.* **1981**, *103*, 5620–5621. Bolinger, C. M.; Hoots, J. E.; Rauchfuss, T. B. *Organometallics* **1982**, *1*, 223–225. Bolinger, C. M.; Rauchfuss, T. B. *Inorg. Chem.* **1982**, *21*, 3947–3954.

(14) Ginsberg, A. P.; Osborne, J. H.; Sprinkle, C. R. *Inorg. Chem.* **1983**, *23*, 254–266 reports an SCF–Xα–SW study of the disulfur and diselenium complexes $[M(X_2)(PH_3)_4]^+$ (M = Rh, Ir; X = S, Se)).

0020-1669/83/1322-1781$01.50/0

component of this transition may be described as Se_2 $\pi^* \rightarrow$ Se_2 $p\sigma^*$, where Se_2 refers to the two central selenium atoms of the Se_4 group. It is thus analogous to the HOMO $\rightarrow$ LUMO transition of $[Ir(Se_2)(dppe)_2]^+$, which occurs at 590 nm and for which the largest single component is Se_2 $\pi^*_\perp \rightarrow$ Se_2 $p\sigma^*$.[14]

Experimental Section

Unless otherwise indicated, all procedures were carried out by Schlenk techniques under a nitrogen or argon atmosphere or in a He-filled Vacuum Atmospheres drybox equipped with a recirculating system. Reagent grade solvents were distilled under nitrogen after drying. Benzene, tetrahydrofuran, and acetonitrile were dried, respectively, with sodium wire, lithium aluminum hydride, and calcium hydride. $[Ir(dmpe)_2]Cl$ was prepared by refluxing $[(IrCl(C_8H_{14})_2)_2]$ with the stoichiometric amount of dmpe in benzene solution. Monoclinic red selenium was obtained by CS_2 Soxhlet extraction of the product from the SO_2 reduction of selenous acid. Melting points were determined in evacuated tubes and are uncorrected. Microanalyses were performed by the Analytische Laboratorien, Engelskirchen, West Germany.

Conductivity measurements were made with a Serfass conductivity bridge at 25.0 ± 0.1 °C; samples were in acetonitrile solution and spanned the concentration range 10^{-2}–10^{-4} mequiv/mL. The conductivity cell, consisting of two 1 cm^2 platinized platinum electrodes separated by ~1 cm, was calibrated with 0.10 M KCl solution. Infrared spectra (4000–250 cm^{-1}) were recorded with a Perkin-Elmer 457 spectrophotometer using samples in pressed CsI disks. Electronic absorption spectra (300–700 nm) were measured with a Cary Model 14R spectrophotometer using samples of concentration (1×10^{-3})–(1×10^{-5}) M in EPA glass at liquid-nitrogen temperature. The glass samples were prepared as described previously[14] and had an effective path length of 3.45 cm. Extinction coefficients were corrected for solvent contraction by multiplying by 0.771, the fractional change in volume of EPA on cooling from +20 to −196 °C.[15]

Reaction of $[Ir(dmpe)_2]Cl$ with Se_8. Monoclinic red selenium (1.73 g, 2.74 mmol of Se_8) was added to a suspension of $[Ir(dmpe)_2]Cl$ (1.91 g, 3.62 mmol) in 1:1 tetrahydrofuran–benzene (100 mL), and the mixture was stirred at room temperature in the dark for 8 days. The suspended solid was filtered off and extracted with acetonitrile (6 × 30 mL). After concentration to 100 mL, the dark brown extract was transferred onto a 1.5 × 32 cm column of acid alumina (Woelm, activity I) open to the air. Elution with neat acetonitrile caused no significant movement of the absorbed material. Elution with acetonitrile containing 1% CH_3OH gave successively yellow, purple, and red fractions. The yellow fraction contained only a small amount of dissolved material and was discarded. Evaporation of the purple fraction to dryness and recrystallization of the residue from acetonitrile–ether under anhydrous conditions gave deep purple $[Ir(Se_2)(dmpe)_2]Cl$ (175 mg, 7%, after drying at 100 °C (10^{-3} mm)), mp 311–312 °C dec. Anal. Calcd for $C_{12}H_{32}P_4IrSe_2Cl$: C, 21.01; H, 4.70; P, 18.06; Cl, 5.17; Se, 23.03. Found: C, 20.85; H, 4.50; P, 17.88; Cl, 5.24; Se, 23.36. Under a polarizing microscope with transmitted light the microcrystalline compound is pleochroic, changing from purple to green as the stage is rotated. By reflected light the crystals appear black.

Evaporation of the red fraction to dryness and recrystallization of the residue from acetonitrile–toluene under anhydrous conditions and in subdued light gave deep red crystalline $[Ir(Se_4)(dmpe)_2]Cl$ (1.06 g, 35%, after drying at 100 °C (10^{-3} mm)), mp 277–280 °C dec. Anal. Calcd for $C_{12}H_{32}P_4IrSe_4Cl$: C, 17.08; H, 3.82; P, 14.68; Cl, 4.20; Se, 37.43. Found: C, 17.16; H, 3.75; P, 14.65; Cl, 4.19; Se 37.18.

Reaction of $[Ir(Se_4)(dmpe)_2]Cl$ with PPh_3. A solution of PPh_3 (18 mg, 0.069 mmol) in acetonitrile (5 mL) was mixed with an acetonitrile (15 mL) solution of $[Ir(Se_4)(dmpe)_2]Cl$ (29 mg, 0.034 mmol). after 15 min, the initially reddish yellow solution had become pink and after overnight standing was pale purple. Acetonitrile was removed under reduced pressure, and the residue was extracted with toluene (3 × 3 mL). The remaining purple solid was washed with diethyl ether and pumped dry; it was identified as $[Ir(Se_2)(dmpe)_2]Cl$ by comparison of its IR (4000–250 cm^{-1}) and visible (300–800 nm) spectra with the spectra of the complex obtained directly from the reaction of Se_8 with $[Ir(dmpe)_2]Cl$; yield 21 mg (90%). Evaporation of the toluene extract to dryness gave a white crystalline solid that was identified as Ph_3PSe from its IR spectrum (ν(PSe) = 560 cm^{-1}).

(15) Passerini, R.; Ross, I. G. *J. Sci. Instrum.* **1953**, *30*, 274.

Table I. Summary of Experimental Details for Determination of the Crystal Structure of $[Ir(Se_4)(dmpe)_2]Cl$

A. Crystal Data

formula: $C_{12}H_{32}ClIrSe_4P_4$
fw: 843.78
$F(000)$ = 12608
cryst dimens: 0.10 × 0.14 × 0.18 mm
peak width at half-height: 0.20°
radiation: Mo Kα (λ = 0.71073 Å)
temp = 23 ± 1 °C
cryst descripn: orthorhombic, space group *Fddd*
a = 15.406 (5) Å
b = 26.792 (6) Å
c = 50.591 (13) Å
V = 20881.6 Å^3
Z = 32
ρ = 2.15 g/cm^3
μ = 117.5 cm^{-1}

B. Intensity Measurements

instrument: Enraf-Nonius CAD4 diffractometer
monochromator: graphite crystal, incident beam
attenuator: Zr foil, factor 20.7
takeoff angle: 2.8°
detector aperture: 2.0–2.4 mm horizontal, 2.0 mm vertical
cryst-detector dist: 21 cm
scan type: ω–θ
scan rate: 2–20°/min (in ω)
scan width: $(0.6 + 0.350 \tan \theta)°$
max 2θ: 48.0°
no. of reflctns measd: 4550 total, 4101 unique
corrections: Lorentz-polarization, linear decay (from 1.00 to 1.02 on I) empirical abs (from 0.76 to 0.99 on I)

C. Structure Solution and Refinement

solution: direct methods
hydrogen atoms: not included
refinement: full-matrix least squares
minimization function: $\Sigma w(|F_o| - |F_c|)^2$
least-squares wts: $4F_o^2/\sigma^2(F_o^2)$
"ignorance" factor: 0.070
anomalous dispersion: all non-hydrogen atoms
reflctns included: 1934 with $F_o^2 > 3.0\sigma(F_o^2)$
parameters refined: 144
unweighted agreement factor: 0.056
weighted agreement factor: 0.075
factor including unobsd data: 0.185
esd of observn of unit wt: 1.44
convergence, largest shift: 0.13σ
high peak in final diff map: 1.71 (2) e/Å^2
computer hardware: PDP-11/45
computer software: Enraf-Nonius SDP and private programs of Molecular Structure Corp.

Determination of the Structure of $[Ir(Se_4)(dmpe)_2]Cl$.[16] Single crystals suitable for X-ray diffraction were obtained by vapor diffusion of benzene into a solution of $[Ir(Se_4)(dmpe)_2]Cl$ (50 mg) in acetonitrile (12 mL). Table I summarizes the experimental details for data collection and reduction and for solution and refinement of the structure.

A red prismatic crystal (0.10 × 0.14 × 0.18 mm) of the complex was mounted on a glass fiber with its long axis roughly parallel to the φ axis of the goniometer. All data were collected on an Enraf–Nonius CAD4 diffractometer using Mo Kα radiation. Unit cell constants were obtained by least-squares refinement of the setting angles of 25 computer-centered reflections in the range $3 < \theta < 17°$; the results are given in Table I. From the systematic absences of

hkl: $h + k$, $k + l$, $h + l = 2n + 1$ $\quad 0kl$: $k + l = 4n + 1$
$h0l$: $h + l = 4n + 1$ $\quad hk0$: $h + k = 4n + 1$

and from subsequent least-squares refinement, the space group was determined to be orthorhombic *Fddd* (No. 70).

(16) This structure determination was performed by the crystallographic staff of Molecular Structure Corp.: Dr. M. W. Extine, Ms. R. A. Meisner, and Dr. J. M. Troup.

Table II. Final Positional Parameters for the Non-Hydrogen Atoms of $[Ir(Se_4)(dmpe)_2]Cl$[a,b]

atom	x	y	z
Ir1	0.1250	0.12500	0.02731 (2)
Ir2	0.1250	0.45155 (5)	0.12500
Se1	0.1285 (2)	0.05638 (9)	−0.00752 (5)
Se2	0.0811 (2)	0.09024 (1)	−0.04763 (5)
Se3	0.2352 (2)	0.38663 (1)	0.11029 (6)
Se4	0.1974 (3)	0.31038 (1)	0.12800 (9)
Cl1	0.3256 (6)	0.1250	0.1250
P1	0.1351 (7)	0.1904 (3)	0.0571 (1)
P2	0.2769 (5)	0.1238 (3)	0.0279 (1)
P3	0.2338 (5)	0.5110 (3)	0.1200 (1)
P4	0.1727 (6)	0.4490 (3)	0.1688 (1)
Cl2A	0.302 (2)	0.384 (1)	0.2905 (7)
Cl2B	0.537 (3)	0.542 (2)	0.4970 (8)
C1	0.116 (2)	0.251 (1)	0.0472 (7)
C2	0.110 (3)	0.186 (2)	0.0921 (8)
C3	0.257 (4)	0.202 (2)	0.0628 (1)
C4	0.319 (3)	0.174 (2)	0.0456 (9)
C5	0.335 (2)	0.134 (1)	−0.0036 (7)

[a] Estimated standard deviations in the least significant digits are shown in parentheses. [b] Atoms Cl2A and Cl2B were refined at 0.25 occupancy.

As a check on crystal and electronic stability three representative reflections were measured every 41 min during data collection. The results indicated a total loss in intensity of 2.1%. A linear decay correction was therefore applied to the data, with correction factors on I ranging from 1.00 to 1.02, with an average value of 1.01. The data were also corrected for absorption, Lorentz, and polarization effects. The structure was solved by direct methods and difference Fourier synthesis and was then refined by the full-matrix least-squares method. Hydrogen atoms were not included in the calculations. A list of the observed and calculated structure factors is available.[17]

Procedure for Molecular Orbital Calculations

SCF–Xα–SW calculations[18,19] were carried out in single precision on a Cray-1 computer using revised versions[20] of the programs written originally by K. H. Johnson and F. C. Smith. The program package includes code by J. H. Wood and A. M. Boring, which applies relativistic mass–velocity and Darwin corrections to the calculations.[21]

Figure 1 shows the coordinate axes, conformation, and atom numbering for the C_2 model complex $[Ir(Se_4)(PH_3)_4]^+$. Coordinates in atomic units (1 bohr = 0.52917 Å) were derived from the averaged bond distances and angles found in the structure of $[Ir(Se_4)(dmpe)_2]Cl$ (Tables III and IV) and from d(P–H) and ∠H–P–H in the PH_3 molecule.[22] Overlapping atomic sphere radii were taken as 88% of the atomic number radii;[23] the values are as follows (in bohrs): Ir, 2.5886; Se1, 2.6961; Se2, 2.6134; P_{ax}, 2.3308; P_{eq}, 2.3342; H1, 1.4617; H2, 1.4602; H3, 1.4618; H4, 1.4613; H5, 1.4608; H6, 1.4619. These values gave a satisfactory virial ratio ($-2T/V$ = 1.000062 for the nonrelativistic calculation). The outer sphere surrounding the molecule was centered at the valence electron weighted average of the atom positions and was taken tangent to the Se2 spheres, giving an outer sphere radius of 9.0176 bohrs. A Watson sphere,[24] bearing a 1− charge and having the same radius and center as the outer sphere, was used to simulate the electrostatic interaction of the complex with its surrounding crystal lattice. α exchange-correlation parameter values

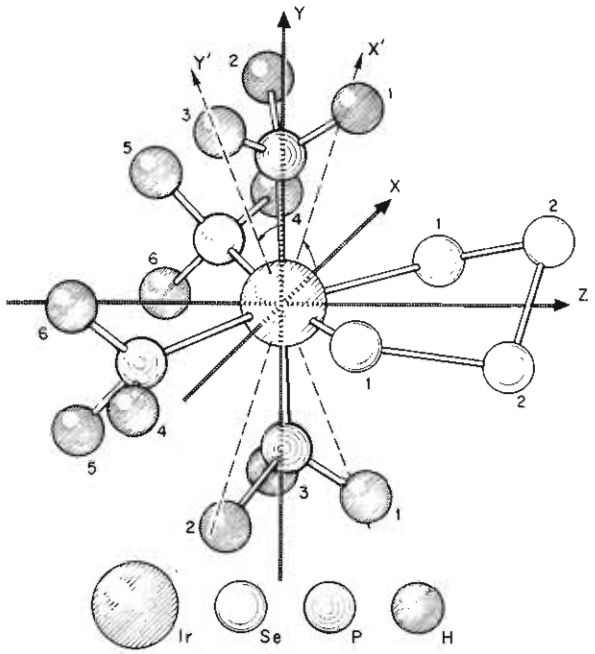

Figure 1. Coordinate axes and atom-labeling scheme for $[Ir(Se_4)(PH_3)_4]^+$ (C_2). The $x'y'z$ coordinate system is obtained from the xyz system by a 34.63° CCW rotation about the z axis; the x' axis is parallel to the Se2–Se2 bond.

were as follows:[25,26] α_{Ir} = 0.69296, α_{Se} = 0.70638, α_P = 0.72620, α_H = 0.77725. In the extramolecular and intersphere regions α was taken as an average of the atomic sphere α values weighted by the number of valence electrons in the neutral atoms, giving $\alpha_{OUT} = \alpha_{INT}$ = 0.72370.

The intial cluster potential for $[Ir(Se_4)(PH_3)_4]^+$ was constructed by superposing SCF–Xα charge densities for Ir^+, Se^0, P^0, and H^0. Partial waves through l = 5 in the extramolecular region, l = 3 in the iridium sphere, l = 2 in the selenium and phosphorus spheres, and l = 0 in the hydrogen spheres were used to expand the wave functions. C_2 symmetry was used to factor the secular matrix. The spin-restricted nonrelativistic ground-state calculations required about 50 s of Cray-1 processor time/iteration and were carried through 25 iterations before relativistic effects were included. An additional 29 iterations (ca. 1 min/iteration) were required to converge the relativistic calculation to ±0.0001 Ry or better for the valence levels. A weighted average of the initial and final potential for a given iteration was used as the starting potential for the next iteration; the proportion of final potential in the average was 10–15%.

The final $[Ir(Se_4)(PH_3)_4]^+$ ground-state potential was used to search for virtual levels up to a maximum energy of −0.05 Ry; it also served as the starting point for SCF calculations of the Slater transition states for one-electron transitions to the virtual levels.[18,19] The transition-state calculations were carried out in spin-restricted form to give an estimate of the weighted average of the singlet and triplet transition energies.

Results and Discussion

Synthesis and Reactions. *cyclo*-Octaselenium reacts in the dark at room temperature with $[Ir(dmpe)_2]Cl$ to form, as the major characterizable product, deep red $[Ir(Se_4)(dmpe)_2]Cl$ together with small amounts of deep purple $(Ir(Se_2)(dmpe)_2]Cl$. The purple compound is undoubtedly a side-on-bonded Se_2 complex, analogous to the known $[Rh(Se_2)(dmpe)_2]Cl$:[11] Both compounds have the same IR spectrum in the 4000–200-cm^{-1} region, and conductivity measurements confirm that the iridium complex is also a 1:1 electrolyte.[27] As described below, a single-crystal X-ray structure deter-

(17) See the supplementary material paragraph at the end of the paper for details.
(18) Slater, J. C. "The Self-Consistent Field for Molecules and Solids: Quantum Theory of Molecules and Solids"; McGraw-Hill: New York, 1974; Vol. 4.
(19) Slater, J. C. "The Calculation of Molecular Orbitals"; Wiley: New York, 1979.
(20) Locally modified version of the revision by Mike Cook, Bruce Bursten, and George Stanly.
(21) Wood, J. H.; Boring, A. M. *Phys. Rev. B: Condens. Matter* **1978**, 18, 2701.
(22) Kuchitsu, K. *J. Mol. Spectrosc.* **1961**, *7*, 399. Sirvetz, M. H.; Weston, R. E. *J. Chem. Phys.* **1953**, *21*, 898.
(23) Norman, J. G., Jr. *Mol. Phys.* **1976**, *31*, 1191.
(24) Watson, R. E. *Phys. Rev.* **1958**, *111*, 1108.
(25) Schwarz, K. *Phys. Rev. B: Solid State* **1972**, *5*, 2466. Schwarz, K. *Theor. Chim. Acta* **1974**, *34*, 225.
(26) Slater, J. C. *Int. J. Quantum Chem., Symp.* **1973**, *7*, 533.
(27) Conductivity measurements on acetonitrile solutions of $[Ir(Se_2)(dmpe)_2]Cl$ give a linear Λ_e vs. $c^{1/2}$ plot, with slope A_{obsd} = 373 compared to $A(1:1)_{theory}$ = 342; Λ_o = 152.

Table III. Bond Distances (Å) for $[Ir(Se_4)(dmpe)_2]Cl$[a]

atom 1	atom 2	dist	atom 1	atom 2	dist	atom 1	atom 2	dist
Ir1	Se1	2.547 (2)	P1	C3	1.93 (5)	Ir2	P4	2.337 (6)
Ir1	Se1	2.547 (2)	P2	C4	1.74 (4)	Se3	Se4	2.305 (4)
Ir1	P1	2.318 (6)	P2	C5	1.85 (3)	Se4	Se4	2.251 (7)
Ir1	P1	2.318 (6)	P2	C6	1.72 (4)	P3	C7	1.87 (3)
Ir1	P2	2.340 (6)	C3	C4	1.50 (5)	P3	C8	1.87 (3)
Ir1	P2	2.340 (6)	Ir2	Se3	2.542 (3)	P3	C9	1.85 (3)
Se1	Se2	2.340 (3)	Ir2	Se3	2.542 (3)	P4	C10	1.83 (3)
Se2	Se2	2.301 (5)	Ir2	P3	2.325 (6)	P4	C11	1.86 (3)
P1	C1	1.74 (3)	Ir2	P3	2.325 (6)	P4	C12	1.87 (3)
P1	C2	1.81 (4)	Ir2	P4	2.337 (6)	C9	C10	1.56 (3)

[a] Numbers in parentheses are estimated standard deviations in the least significant digits.

Table IV. Bond Angles (deg) for $[Ir(Se_4)(dmpe)_2]Cl$[a]

atom 1	atom 2	atom 3	angle	atom 1	atom 2	atom 3	angle	atom 1	atom 2	atom 3	angle
Se1	Ir1	Se1	92.5 (1)	C1	P1	C3	94 (2)	P3	Ir2	P4	98.3 (2)
Se1	Ir1	P1	174.1 (2)	C2	P1	C3	94 (2)	P3	Ir2	P4	98.3 (2)
Se1	Ir1	P1	84.6 (2)	Ir1	P2	C4	112 (1)	P3	Ir2	P4	84.0 (2)
Se1	Ir1	P2	88.7 (2)	Ir1	P2	C5	118 (1)	P4	Ir2	P4	176.7 (3)
Se1	Ir1	P2	92.3 (2)	Ir1	P2	C6	113 (1)	Ir2	Se3	Se4	108.9 (1)
Se1	Ir1	P1	84.6 (2)	C4	P2	C5	99 (2)	Se3	Se4	Se4	101.4 (2)
Se1	Ir1	P1	174.1 (2)	C4	P2	C6	108 (2)	Ir2	P3	C7	117.4 (9)
Se1	Ir1	P2	92.3 (2)	C5	P2	C6	106 (2)	Ir2	P3	C8	123.6 (9)
Se1	Ir1	P2	88.7 (2)	P1	C3	C4	117 (4)	Ir2	P3	C9	107.5 (9)
P1	Ir1	P1	98.8 (3)	P2	C4	C3	117 (3)	C7	P3	C8	102 (1)
P1	Ir1	P2	86.3 (3)	Se3	Ir2	Se3	93.6 (1)	C7	P3	C9	101 (1)
P1	Ir1	P2	92.8 (3)	Se3	Ir2	P3	87.5 (2)	C8	P3	C9	102 (1)
P1	Ir1	P2	92.8 (3)	Se3	Ir2	P3	168.9 (2)	Ir2	P4	C10	109 (1)
P1	Ir1	P2	86.3 (3)	Se3	Ir2	P4	92.8 (2)	Ir2	P4	C11	120.9 (9)
P2	Ir1	P2	178.6 (3)	Se3	Ir2	P4	85.0 (2)	Ir2	P4	C12	118 (1)
Ir1	Se1	Se2	108.3 (1)	Se3	Ir2	P3	168.9 (2)	C10	P4	C11	101 (1)
Se1	Se2	Se2	97.5 (1)	Se3	Ir2	P3	87.5 (2)	C10	P4	C12	105 (1)
Ir1	P1	C1	121 (1)	Se3	Ir2	P4	85.0 (2)	C11	P4	C12	100 (1)
Ir1	P1	C2	125 (1)	Se3	Ir2	P4	92.8 (2)	P3	C9	C10	108 (2)
Ir1	P1	C3	106 (2)	P3	Ir2	P3	93.6 (3)	P4	C10	C9	109 (2)
C1	P1	C2	108 (2)	P3	Ir2	P4	84.0 (2)				

[a] Numbers in parentheses are estimated standard deviations in the least significant digits.

mination has shown that the $[Ir(Se_4)(dmpe)_2]Cl$ crystal lattice is made up of $[Ir(Se_4)(dmpe)_2]^+$ cations and Cl^- anions. However, conductivity measurements on acetonitrile solutions of $[Ir(Se)_4(dmpe)_2]Cl$ give a linear Λ_e vs. $c^{1/2}$ plot with a slope (A) significantly higher than expected for a 1:1 electrolyte ($A_{obsd} = 616$, $A(1{:}1)_{theory} = 349$, $A(2{:}1)_{theory} = 674$; $\Lambda_o = 161$), suggesting that the complex is associated in solution. The formation of an Se_4 complex as the major product of the reaction between Se_8 and $[Ir(dmpe)_2]Cl$ is surprising in view of the fact that only the side-on-bonded Se_2 and S_2 complexes have been obtained from the reaction of $[Rh(dmpe)_2]Cl$ and $[Ir(dppe)_2]Cl$ with Se_8 and S_8.[11]

$[Ir(Se_4)(dmpe)_2]Cl$ is soluble in ethanol, acetonitrile, nitromethane, nitrobenzene, methylene chloride, and chloroform; it is insoluble in tetrahydrofuran, diethyl ether, and hydrocarbons. Solutions of the complex deposit red selenium on exposure to fluorescent light or sunlight but are stable in the dark. The complex is somewhat hygroscopic but is otherwise air stable. $[Ir(Se_4)(dmpe)_2]Cl$ is readily converted to $[Ir(Se_2)(dmpe)_2]Cl$ by treatment with PPh_3 in acetonitrile solution:

$$[Ir(Se_4)(dmpe)_2]Cl + 2PPh_3 \xrightarrow[CH_3CN]{} [Ir(Se_2)(dmpe)_2]Cl + 2Ph_3PSe$$

Crystal Structure of $[Ir(Se_4)(dmpe)_2]Cl$. Table II lists the final positional parameters (thermal parameters may be found in a supplementary table[17]), and Tables III and IV summarize the bond distances and angles in the cation. There are two unique $[Ir(Se_4)(dmpe)_2]^+$ cations in the structure; each lies on a crystallographic 2-fold axis. One of the Cl^- anions also is on a 2-fold axis; the other chloride is disordered, appearing at two different general positions.[28] Figure 2 is a perspective drawing of the two cations that shows the atom-numbering scheme and some important bond distances and angles.

The inner coordination geometry about Ir1 and Ir2 is distorted *cis* octahedral, with the Se_4 group symmetrically chelated to the iridium at equatorial positions and each dmpe group chelating axial and equatorial positions. There are no significant differences between the Ir–P or between the Ir–Se bond distances in the two unique cations. The conformation of the $IrSe_4$ ring is analogous to the "half-chair" form of the cyclopentane ring: The two central selenium atoms of the Se_4 group are at equal distances from and on opposite sides of the plane containing the Ir atom and the two coordinated Se atoms. In the Ir1 cation, the out-of-plane selenium atoms (Se2) are 0.702 Å distant from the Ir–Se1–Se1 plane while in the Ir2 cation, the distance from the Ir–Se3–Se3 plane to the Se4 atoms is significantly less at 0.587 Å. Both cations show a small but statistically significant alternation of the Se–Se bond distances in the $IrSe_4$ ring, the central bond being in each case 0.04–0.05 Å shorter than the two outer bonds. However, the central bond distance Se2–Se2 in the Ir1 cation is not significantly different from the outer bond distance Se3–Se4 in the Ir2 cation. A "half-chair" conformation is also assumed by the Ir2–P3–C9–C10–P4 rings, which have C9 and C10 on opposite sides of the Ir2–P3–P4 plane (C9 and C10 are respectively −0.53 and +0.22 Å distant from the plane). The corresponding rings in the Ir1 cation, Ir1–P1–C3–C4–P2, have the "envelope" configuration, with both C3 and C4 on

(28) There also appears to be some disorder in the P1–C3–C4 moiety, as evidenced by the larger thermal parameters and somewhat unusual bond distances for these atoms.

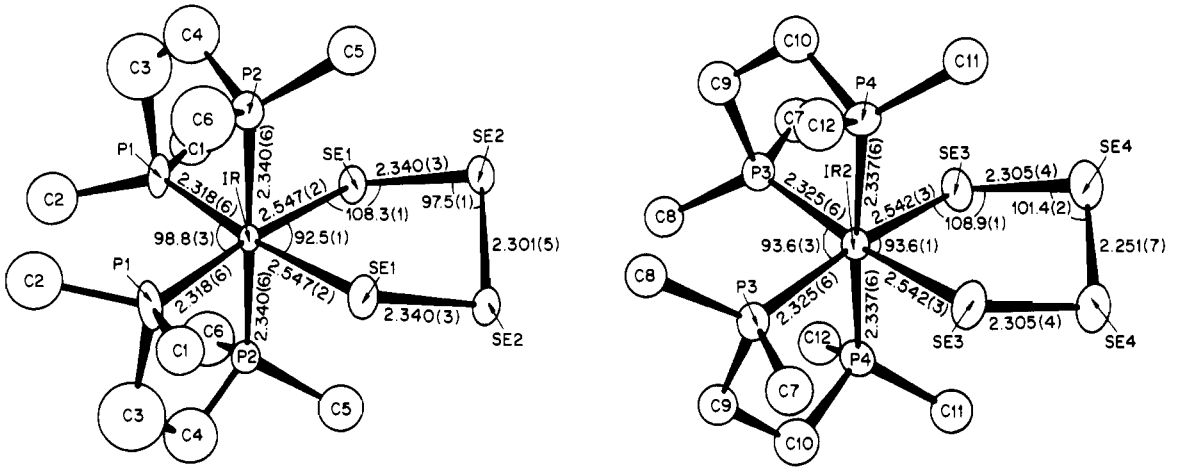

Figure 2. Perspective view of the two unique $[Ir(Se_4)(dmpe)_2]^+$ cations showing the atom-numbering scheme and some important bond distances and angles. Thermal motion is represented by 50% probability ellipsoids or spheres.

the same side of the Ir1–P1–P2 plane (C3 is only 0.02 Å distant from the plane while C4 is further away at a distance of 0.21 Å).

Both the Ir–Se and Se–Se bond distances found for $[Ir(Se_4)(dmpe)_2]^+$ are very similar to the values found for the diselenium complex $[Ir(Se_2)(dppe)_2]^+$[11] (compare mean Ir–Se = 2.53 Å and Se–Se = 2.312 Å in the Se_2 complex), which also has cis-octahedral coordination about the iridium atom. Compared to the free Se_2 molecule (Se–Se distance 2.19 (3) Å[29]) the coordinated Se_4 group has 0.06–0.15 Å longer Se–Se bonds. We may compare the conformation of the $IrSe_4$ ring with the conformation of MS_4 rings in complexes containing the chelated S_4 group. Both half-chair and envelope conformations have been found for MS_4 rings. The half-chair conformation occurs in $(\eta^5\text{-}C_5H_5)_2MS_4$ (M = Mo, W),[3,4] where the central sulfur atoms are disposed at approximately equal distances on opposite sides of the plane containing the metal and two coordinated S atoms; for $(\eta^5\text{-}C_5H_5)_2MoS_4$ the distances are 0.53 and 0.65 Å. Alternation of S–S bond lengths, with the central S–S bond significantly shorter than the terminal S–S bonds, has been observed for coordinated S_4 in both the half-chair and envelope conformations. In the case of $(\eta^5\text{-}C_5H_5)_2MoS_4$ the central S–S bond is 0.07 Å shorter than the outer bonds, a shortening similar to what we have found for coordinated Se_4. In the other structures that have been reported, the shortening of the central S–S bond, as compared to the outer S–S bonds, is considerably greater.[6] S–S bond length alternation does not occur in the uncoordinated S_4^{2-} group.[30]

The Ir–P distances found for the Se_4 complex are very similar to the values found for $[Ir(Se_2)(dppe)_2]^+$[11] and related complexes. Like these compounds, $[Ir(Se_4)(dmpe)_2]^+$ has slightly longer axial than equatorial Ir–P bonds.

Electronic Structure of $[Ir(Se_4)(PH_3)_4]^+$. The calculated ground-state one-electron energies, charge distributions, and partial wave analyses for the valence molecular orbitals of $[Ir(Se_4)(PH_3)_4]^+$ are summarized in Table VI; the basis function notation is explained in Table V. Note that the 2 Se2 basis functions refer to the $x'y'z$ coordinate system in Figure 1, while the Ir and 2 Se1 functions refer to the xyz coordinate system. Figure 3 is a diagram of the valence energy levels, which includes for comparison the energy levels of $[Ir(Se_2)(PH_3)_4]^+$.[14] Wave function contour maps of selected orbitals are shown in Figures 4, 5, and 7. Total valence charge density contour maps are exhibited in Figure 6.

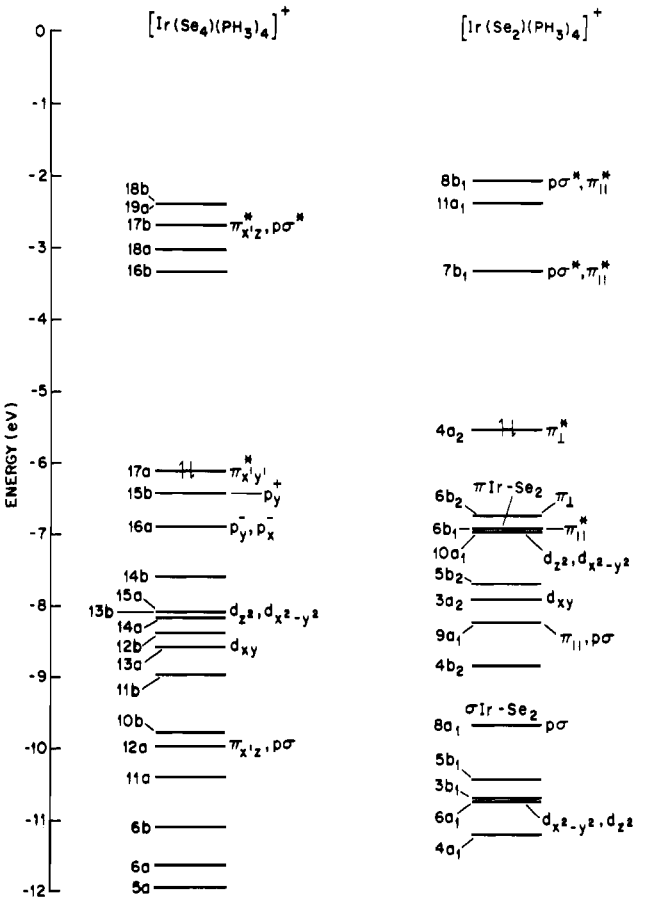

Figure 3. SCF valence energy levels for $[Ir(Se_4)(PH_3)_4]^+$ and $[Ir(Se_2)(PH_3)_4]^+$ above −15 eV. Purely PH_3 P–H bonding orbitals have been omitted from the diagram. The highest occupied level is marked by paired arrows. Levels in which there is a relative charge of 50% or more in the Ir, 2 Se1, or 2 Se2 atomic spheres are labeled with the spherical harmonic basis functions which contribute at least 20% of the charge in that region. The results for $[Ir(Se_2)(PH_3)_4]^+$ are from ref 14.

Table VII gives the calculated total charge distribution as well as estimated net atomic charges. The absolute values of the net atomic charges may not be reliable since they depend on a rather crude method of assigning the intersphere and extramolecular charge to the atomic spheres (cf. footnote *a*, Tables VI and VII). However, we believe that comparisons of these net atomic charges with charges calculated in the same way for similar complexes, in particular $[Ir(Se_2)(PH_3)_4]^+$, are

(29) Maxwell, L. R.; Mosley, V. M. *Phys. Rev.* **1940**, *57*, 21.
(30) Abrahams, S. C.; Bernstein, J. L. *Acta Crystallogr., Sect B* **1969**, *B25*, 2365–2370.

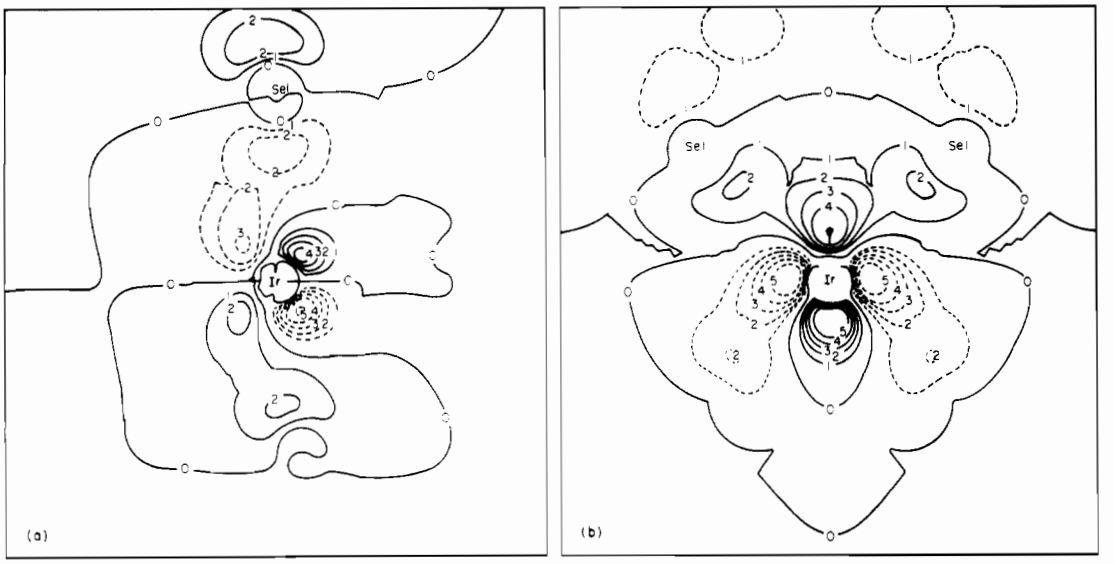

Figure 4. Wave function contour maps of the main Ir–Se bonding orbitals in $[Ir(Se_4)(PH_3)_4]^+$: (a) Level 14b in the plane through Ir, Sel, and the y axis (there is an analogous map in the corresponding plane through the second Ir–Sel bond); (b) Level 14a in the plane through Ir and 2 Sel. Solid and broken lines denote contours of opposite sign having magnitudes indicated by the numerical labels 0, 1, 2, 3, 4, 5 = 0, 0.05, 0.075, 0.10, 0.125, 0.16 [electron/(bohr)^3]$^{1/2}$, respectively. Contours close to atomic centers are omitted for clarity.

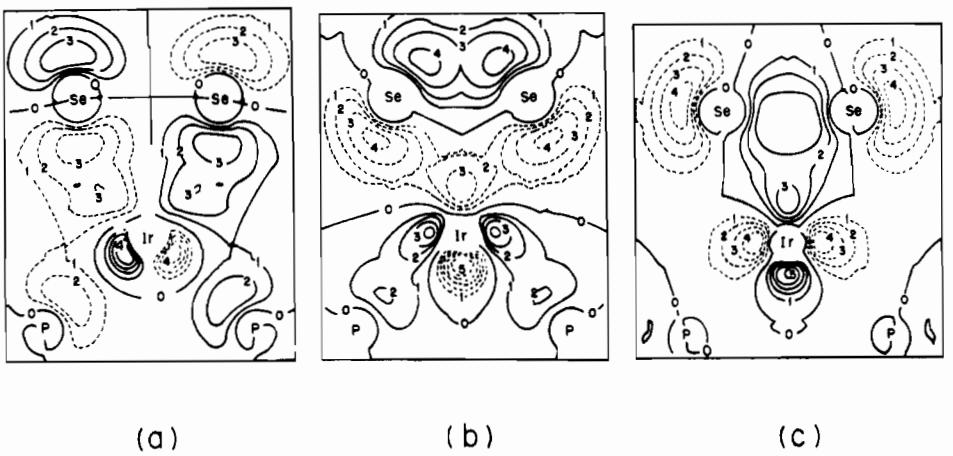

Figure 5. Wave function contour maps of the main Ir–Se bonding orbitals in $[Ir(Se_2)(PH_3)_4]^+$ (from ref 14): (a) level $6b_1$; (b) level $9a_1$; (c) level $8a_1$. Contour magnitudes and sign convention are as in Figure 4. All maps are in the xz plane.

reliable. Similarly, the orbital occupancies given in Table VIII must be regarded as approximate, but comparisons with similarly calculated values for related complexes should be reliable.

The occupied valence molecular orbitals of $[Ir(Se_4)(PH_3)_4]^+$ have energies in the range −21 to −6 eV. Level 17a, the HOMO, is almost entirely localized on the Se_4 group and is both Se2–Se2 and Sel–Se2 antibonding in character. Level 15b, immediately below the HOMO, is also largely localized on the Se4 group; it is weakly antiboding between Sel and Se2 and weakly bonding between Se2 and Se2. In general, however, the ligand and metal orbitals are extensively mixed in the MO's, and it is not possible to identify a set of five predominantly 5d orbitals as would be expected in a ligand-field model. Level 13a, which may be described as predominantly nonbonding $Ir5d_{xy}$ in character, comes the closest to being a ligand-field type orbital. All but three of the levels with significant metal character are to be found in the group of eight orbitals between −6.8 and −9 eV; these include all of the important Ir–Se bonding orbitals. The three levels with important metal character that do not occur in this group are the M–P bonding orbitals 6b, 6a, and 5a, which fall between −11 and −12 eV.

In addition to the occupied levels, Table VI and Figure 3 show five virtual levels, 16b, 18a, 17b, 19a, and 18b. The LUMO, 16b, has 52% of its charge on the Se4 group, 30% in the Ir sphere, and 15% in the equatorial phosphorus spheres. Contour maps show that it is Ir–Sel, Se2–Se2, and Ir–P_{eq} antibonding in character. Levels 18a and 17b are almost entirely localized on the Se_4 group; 18a is mainly Sel–Se2 antibonding while 17b is both Se2–Se2 and Sel–Se2 antibonding. Of the two remaining virtual orbitals, 19a is mainly Ir–P_{ax} antibonding while 18b is mostly Se2–Se2 antibonding.

Examination of contour maps shows that orbitals 14b and 14a make the greatest individual contributions to Ir–Se bonding. Contour maps of these orbitals are shown in Figure 4. In orbital 14b, Ir–Se covalent interaction occurs via overlap of an Sel p_x^+ (74%), p_z^- (21%) hybrid with an Ir $5d_{yz}$ (74%), $6p_x$ (23%) hybrid. In orbital 14a, the interaction takes place through overlap of an Sel p_z^+ (46%), p_x^- (24%), p_y^- (23%) hybrid with a hybrid of $5d_{z^2}$ (49%), $5d_{x^2-y^2}$ (21%), $5d_{xy}$ (20%), $6p_z$ (9%) on Ir. Orbitals 14a and 14b have their largest Ir–Se overlap in orthogonal planes.

It is interesting to compare the Ir–Se covalent bonding in $[Ir(Se_4)(PH_3)_4]^+$ with what was found in $[Ir(Se_2)(PH_3)_4]^+$.[14] In the latter complex three orbitals, $6b_1$, $9a_1$, and $8a_1$, make important contributions to the Ir–Se_2 interaction. Contour maps of these orbitals are shown in Figure 5. Comparing the maps in Figures 4 and 5, we see that the Ir–Se_4 interaction in level 14b resembles the Ir–Se_2 interaction in level $6b_1$ (note that the map of level 14b shows only half of the orbital; there

Table V. Ir, 2 Se1, and 2 Se2 Spherical Harmonic Basis Functions for C_2 $[Ir(Se_4)(PH_3)_4]^+$

representation	Ir functions	2 Se1 functions[a]	2 Se2 functions[b]
A	s, p_z, d_{z^2}, $d_{x^2-y^2}$, d_{xy}	s^+, p_z^+, p_x^-, p_y^-	$s\sigma$, $\pi_{x'z}$, $p\sigma$, $\pi^*_{x'y'}$
B	p_x, p_y, d_{xz}, d_{yz}	s^-, p_z^-, p_x^+, p_y^+	$s\sigma^*$, $\pi^*_{x'z}$, $p\sigma^*$, $\pi_{x'y'}$

[a] The 2 Se1 basis functions are represented by the constituent atomic orbital symbols with a superscript + or − to indicate a sum or difference combination. Thus, $p_z^+ = (1/2^{1/2})(p_z(Se1) + p_z(Se1'))$, etc. [b] The 2 Se2 basis functions refer to the $x'y'z$ coordinate system (Figure 1). $\pi_{x'z}$ and $\pi^*_{x'z}$ have their nodal planes perpendicular to the $x'z$ plane; $\pi_{x'y'}$ and $\pi^*_{x'y'}$ have their nodal planes perpendicular to the $x'y'$ plane. An asterisk indicates an antibonding combination.

Table VI. Valence Molecular Orbitals of $[Ir(Se_4)(PH_3)_4]^+$

		% contribns[a]											basis functions[b,c]		
level[d]	energy, eV	Ir	2 Se1	2 Se2	2 P_{ax}	2 P_{eq}	2 H1	2 H2	2 H3	2 H4	2 H5	2 H6	Ir	2 Se1	2 Se2
18b	−2.376	17	25	44	1	11	0	0	0	0	1	0	d_{xz}	p_z^-, p_x^+	$p\sigma^*$, $\pi^*_{x'z}$
19a	−2.386	41	17	3	25	9	2	1	1	0	1	1	$d_{x^2-y^2}$, d_{z^2}	p_z^+, p_x^-	
17b	−2.680	1	34	63	0	1	0	0	0	0	0	0		p_z^-, p_x^+	$\pi^*_{x'z}$, $p\sigma^*$, $s\sigma^*$
18a	−3.017	7	45	44	1	3	0	0	0	0	0	0		p_z^+, p_x^-	$\pi_{x'z}$, $\pi^*_{x'y'}$
16b	−3.345	30	20	32	0	15	0	0	0	1	1	1	d_{xz}	p_x^+, p_y^+, s^-	$p\sigma^*$, $\pi^*_{x'z}$
17a	−6.113	5	35	59	0	1	0	0	0	0	0	0		p_y^-	$\pi^*_{x'y'}$, $\pi_{x'z}$
15b	−6.423	9	62	24	4	0	0	0	0	0	0	0		p_y^+	$\pi_{x'y'}$, $\pi^*_{x'z}$
16a	−6.866	21	51	23	1	4	0	0	0	0	0	1	d_{xy}, p_z	p_y^-, p_x^-	$\pi^*_{x'y'}$, $\pi_{x'z}$, $p\sigma$
14b	−7.600	27	35	19	1	13	0	0	1	2	0	2	d_{yz}, p_x	p_x^+, p_z^-	$\pi_{x'y'}$, $\pi^*_{x'z}$
15a	−8.083	53	21	11	0	9	0	0	0	1	3	2	d_{z^2}, $d_{x^2-y^2}$	p_x^-, p_y^-, p_z^+	$\pi_{x'z}$, $\pi^*_{x'y'}$
13b	−8.092	13	32	34	15	3	1	0	1	0	0	0	d_{yz}, p_y, p_x	p_x^+, p_y^+	$\pi^*_{x'z}$, $\pi_{x'y'}$
14a	−8.167	41	26	17	1	10	1	0	1	1	0	1	d_{z^2}, $d_{x^2-y^2}$, d_{xy}	p_z^+, p_x^-, p_y^-	$\pi^*_{x'y'}$, $\pi_{x'z}$, $p\sigma$
12b	−8.378	46	8	2	28	4	0	5	4	0	2	1	d_{yz}, p_y		
13a	−8.571	63	13	8	4	3	0	3	2	1	0	1	d_{xy}	p_x^-, p_y^-	
11b	−8.968	23	24	14	27	0	10	0	0	0	0	0	d_{yz}, p_y	p_y^+	$\pi_{x'y'}$, $\pi^*_{x'z}$
10b	−9.770	5	33	42	2	10	0	2	1	5	0	0		p_z^-, p_x^+	$\pi_{x'y'}$, $\pi^*_{x'z}$
12a	−9.972	5	27	59	1	3	1	0	0	3	1	0		p_x^-, p_z^+	$\pi_{x'z}$, $p\sigma$
11a	−10.397	10	12	27	11	17	1	9	4	0	0	10		p_x^-, s^+, p_y^-, p_z^+	$p\sigma$
10a	−10.625	4	5	10	12	27	0	6	7	0	20	8			
9b	−10.692	3	2	1	24	20	11	16	0	1	7	15			
8b	−10.809	2	1	0	33	12	5	6	26	6	7	0			
9a	−10.878	1	1	1	43	2	31	4	14	1	1	0			
7b	−10.916	1	3	3	10	35	0	4	6	22	8	9			
6b	−11.109	44	11	5	2	25	0	1	2	4	5	0	d_{xz}	p_z^-, p_x^+	
8a	−11.122	10	2	1	3	41	1	0	1	33	4	3			
7a	−11.307	7	1	0	24	22	1	16	7	0	7	15			
5b	−11.357	6	1	0	21	25	15	6	1	1	12	13			
6a	−11.636	37	12	15	17	8	2	0	2	1	4	0	$d_{x^2-y^2}$, d_{z^2}	p_z^+	$p\sigma$, $\pi_{x'z}$
5a	−11.964	27	14	15	23	9	3	3	2	0	2	2	s, d_{z^2}	p_z^+	$p\sigma$, $\pi_{x'z}$
4b	−15.964	3	39	58	0	0	0	0	0	0	0	0		s^-, p_z^-	$s\sigma^*$
3b	−17.426	1	0	0	54	13	9	8	9	2	2	2			
4a	−17.462	3	0	0	32	33	5	5	5	5	5	5			
3a	−17.473	2	47	18	14	8	2	2	2	1	2	1		s^+	$s\sigma$, $p\sigma$, $\pi_{x'z}$
2b	−17.606	2	0	0	13	54	2	2	2	8	9	8			
2a	−18.099	5	20	9	21	26	3	3	3	4	4	4		s^+	
1b	−19.253	1	61	38	0	0	0	0	0	0	0	0		s^-	$s\sigma^*$
1a	−21.031	0	22	77	0	0	0	0	0	0	0	0		s^+	$s\sigma$

[a] Relative atomic sphere charges; these are the relative percentages of the orbital charge in the atomic spheres: $\Sigma_{\text{atomic spheres}}$(relative atomic sphere charges) = 100%. [b] See Table V for basis function notation. [c] When more than 10% of the population of a level is located within the Ir, 2 Se1, or 2 Se2 spheres, the spherical harmonic basis functions contributing more than 10% of the charge in that region are listed in order of decreasing importance. [d] The highest occupied level is 17a.

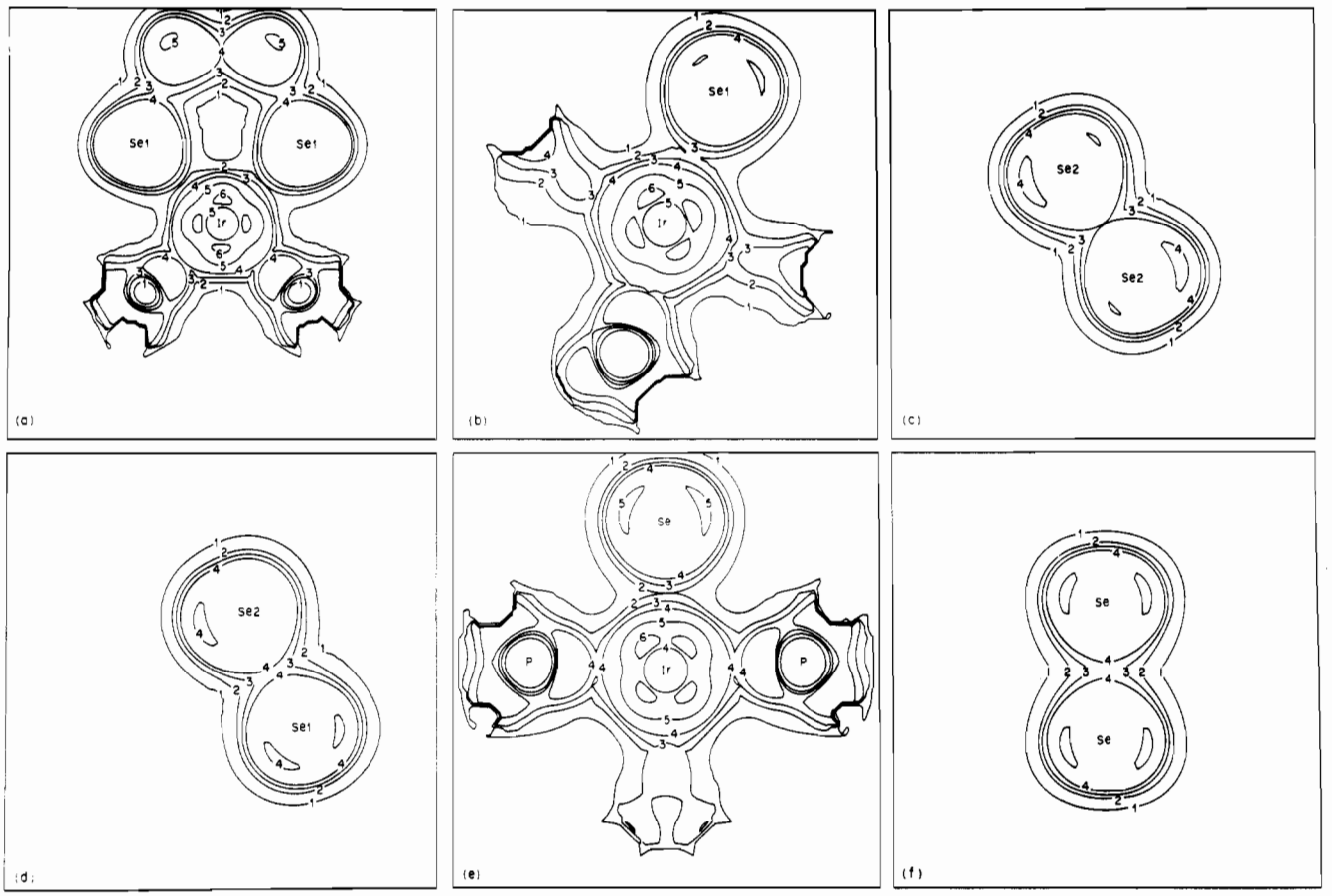

Figure 6. Total valence charge density contour maps for $[Ir(Se_4)(PH_3)_4]^+$ and $[Ir(Se_2)(PH_3)_4]^+$: (a) $[Ir(Se_4)(PH_3)_4]^+$ *xz* plane; (b) $[Ir(Se_4)(PH_3)_4]^+$ plane through Ir, Se1, and the *y* axis; (c) $[Ir(Se_4)(PH_3)_4]^+$ plane through Se2–Se2 and perpendicular to the *z* axis; (d) $[Ir(Se_4)(PH_3)_4]^+$ plane through Se1 and Se2 and parallel to the *y* axis; (e) $[Ir(Se_2)(PH_3)_4]^+$ plane through Ir and Se and parallel to the *y* axis; (f) $[Ir(Se_2)(PH_3)_4]^+$ *xy* plane through Se_2. The contour values are 1, 2, 3, 4, 5, 6, 7 = 0.014, 0.028, 0.035, 0.042, 0.070, 0.140, 0.210 [electron/(bohr)^3]$^{1/2}$, respectively.

Table VII. Total Sphere Charges and Approximate Net Atomic Charges[a] for $[Ir(Se_4)(PH_3)_4]^+$ and $[Ir(Se_2)(PH_3)_4]^+$ [b]

	$[Ir(Se_4)(PH_3)_4]^+$		$[Ir(Se_2)(PH_3)_4]^+$	
sphere	total charge, e	net charge	total charge, e	net charge
Ir	76.71	0.62–	76.67	0.61–
Se1	33.56	0.22–	33.45	0.18–
Se2	33.35	0.09+		
P_{ax}	14.25	0.57+	14.23	0.56+
P_{eq}	14.23	0.61+	14.21	0.63+
H1	1.01	0.05–	1.00	0.05–
H2	1.01	0.04–	1.00	0.03–
H3	1.00	0.03–	1.00	0.03–
H4	1.01	0.04–	0.99	0.03–
H5	1.01	0.04–	1.00	0.03–
H6	1.01	0.04–	1.00	0.03–
INT	4.00		2.86	
OUT	0.37		0.72	

[a] Net atomic charge = atomic no. $- \Sigma_{\text{all levels}}$(relative atomic sphere charge). [b] Results from ref 14.

Table VIII. Approximate Assignment of Valence Electrons to Ir, 2 Sel, and 2 Se2 Basis Functions[a]

basis function	$[Ir(Se_4)(PH_3)_4]^+$		$[Ir(Se_2)(PH_3)_4]^+$ [b]	
5d	8.01		8.00	
6p	0.81		0.80	
6s	0.68		0.69	
s^+	1.82			
s^-	1.86			
p_x^-	1.40			
p_x^+	1.42			
p_z^+	1.04			
p_z^-	1.13			
p_y^-	1.75			
p_y^+	1.69			
sσ	1.86	net sσ = 0.05	1.85	net sσ = −0.03
sσ*	1.81		1.88	
pσ	1.95	net pσ = 1.82	1.98	net pσ = 1.88
pσ*	0.13		0.10	
$\pi_{x'z}$	1.40	net π = 0.43	1.44 ($\pi_\parallel$)	net π = 0.15
$\pi^*_{x'z}$	1.05		1.14 ($\pi_\parallel$)	
$\pi_{x'y'}$	1.64		1.74 ($\pi_\perp$)	
$\pi^*_{x'y'}$	1.56		1.89 ($\pi^*_\perp$)	

[a] See Table V for basis function notation. The values in this table are the contributions of each of the spherical harmonic basis functions to the total valence charge: total valence charge due to BF = $\Sigma_{\text{valence levels}}$(relative atomic sphere charge for level) × (fraction of sphere charge due to BF). [b] Results from ref 14.

is an analogous map for the interaction along the second Ir–Se1 bond) while the interaction in level 14a is similar to that in level $9a_1$. There is no Ir–Se_4 analogue to the σ-Ir–Se_2 overlap in level $8a_1$. The Ir and Se orbitals involved in levels 14a and $9a_1$ are similar (the overlap in level $9a_1$ is between an Se_2 $\pi_\parallel$, pσ hybrid and an Ir $5d_{z^2}$, $5d_{x^2-y^2}$, $6p_z$ hybrid), but levels 14b and $6b_1$ make use of quite different metal hybrid orbitals (level $6b_1$ overlaps an Ir $6p_x$, $5d_{xz}$ hybrid of predominantly p_x character with the Se_2 $\pi^*_\parallel$ orbital). Levels 14b and $6b_1$ also differ in that the $IrSe_4$ level has similar charges on Ir and 2 Sel, while the $IrSe_2$ level has more than twice as much charge on Se_2 as on Ir. The total valence charge density maps in Figure 6 (compare parts a and b of Figure 6 with part e and with Figure 8d of ref 14) indicate that the strength of the covalent Ir–Se interaction is slightly greater in $[Ir(Se_4)(PH_3)_4]^+$ than in $[Ir(Se_2)(PH_3)_4]^+$. The difference is mainly

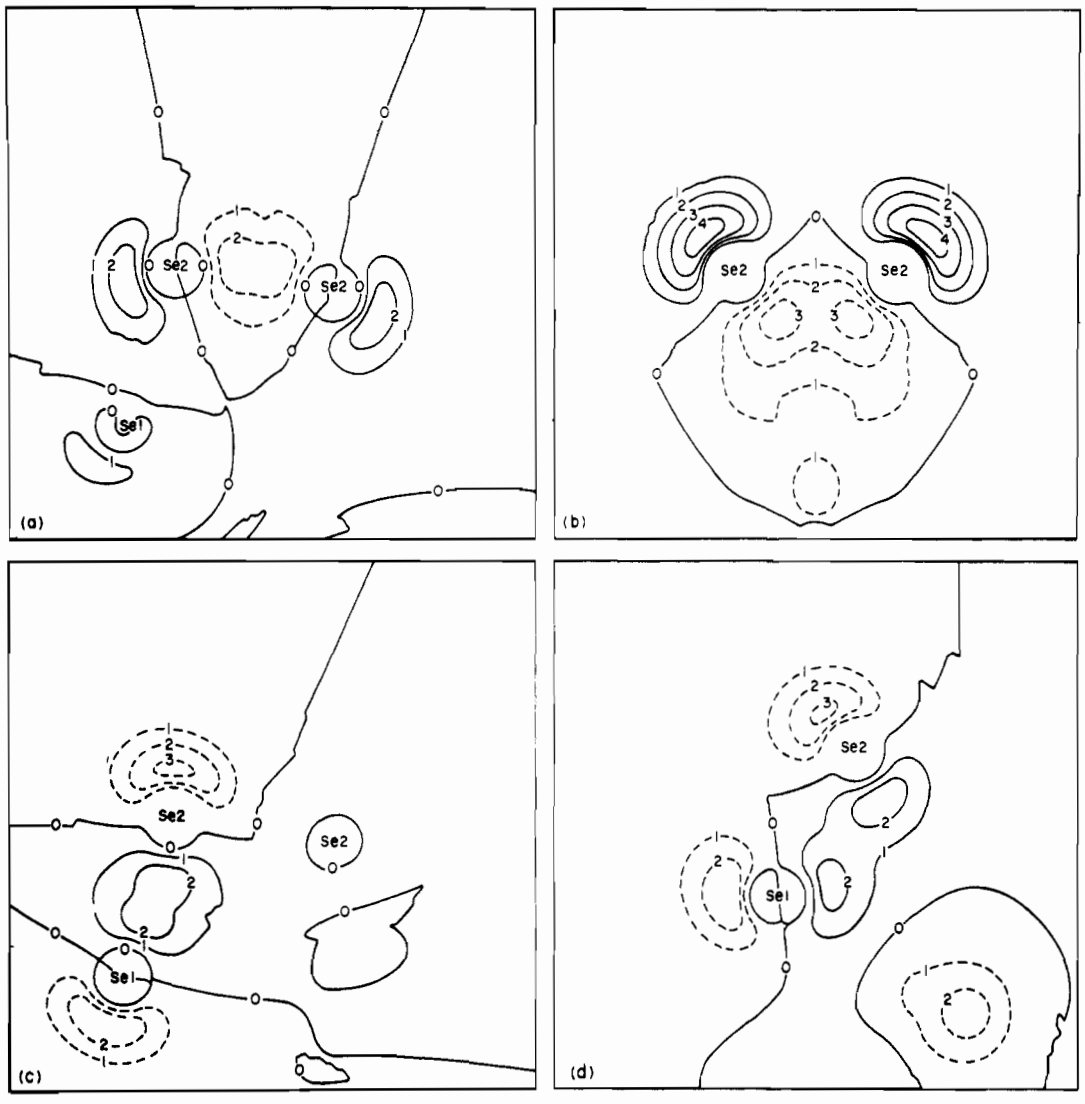

Figure 7. Wave function contour maps of the main Se2–Se2 and Se1–Se2 bonding orbitals in $[Ir(Se_4)(PH_3)_4]^+$: (a) orbital 11a in the Se1, Se2, Se2 plane; (b) orbital 12a in the Ir, Se2, Se2 plane; (c) orbital 10b in the Se1, Se2, Se2 plane; (d) orbital 13b in the plane through Se1–Se2 and parallel to the z axis. Contour magnitudes and sign convention are as in Figure 4.

Table IX. Electronic Absorptions and Assignments for $[Ir(Se_4)(dmpe)_2]Cl$

obsd values[a]				calcd[b]	
λ_{max}, nm	energy, eV	ϵ, M^{-1} cm^{-1}	C_2 transition	energy, eV	atomic character[c]
~450 (sh)	~2.76	~9.3 × 10^2	17a → 16b	2.86	Se2 → Se2, Ir
400 (sh)	3.10	1.2 × 10^3	17a → 18a	3.11	Se2 → Se1, Se2
			15b → 16b	3.17	Se1 → Se2, Ir
363	3.42	2.2 × 10^3	17a → 17b	3.44	Se2 → Se2
			15b → 18a	3.43	Se1 → Se1, Se2
			16a → 16b	3.57	Se1 → Se2, Ir
316	3.92	5.1 × 10^3	15b → 17b	3.82	Se1 → Se2
			16a → 18a	3.89	Se1 → Se1, Se2

[a] Spectrum of sample dissolved in EPA glass at liquid nitrogen temperature, measured from 300 to 800 nm. Extinction coefficients are corrected for solvent contraction on cooling. [b] Spin-restricted transition-state calculation. [c] The major atomic character of the transition; the basis functions involved may be found by reference to Table VI.

due to the greater out-of-plane interaction in the Se_4 complex (cf. Figure 6b,e). In $[Ir(Se_4)(PH_3)_4]^+$ the most important metal orbitals for bonding the Se_4 group are $5d_{yz}$, $5d_{z^2}$ and $6p_x$, while in $[Ir(Se_2)(PH_3)_4]^+$ the Se_2 group is bound mainly via $6p_x$, $5d_{xz}$, $5d_{z^2}$, and $6p_z$.

It is clear from Tables VII and VIII that the net Ir atom charge, as well as the assignment of valence electrons to Ir 5d, 6s, and 6p orbitals, is essentially the same in $[Ir(Se_4)(PH_3)_4]^+$ and $[Ir(Se_2)(PH_3)_4]^+$. Also, the calculated net charge on the Se_4 group (−0.26) is very close to that on the Se_2 group (−0.36). By analogy with the conclusion that the Se_2 group in $[Ir(Se_2)(PH_3)_4]^+$ is best thought of as a neutral molecule in an excited state,[14] we can now say that the Se_4 group in $[Ir(Se_4)(PH_3)_4]^+$ is best described as an excited Se_4 molecule.

From Table VII we see that a $p\sigma$ bond is the major uncanceled Se2–Se2 interaction in the Se4 group. In addition, there is some uncanceled Se2–Se2 π bonding. These interactions occur mainly in levels 11a and 12a and may be seen in the contour maps in Figure 7a,b. A bond order of 1.15 is

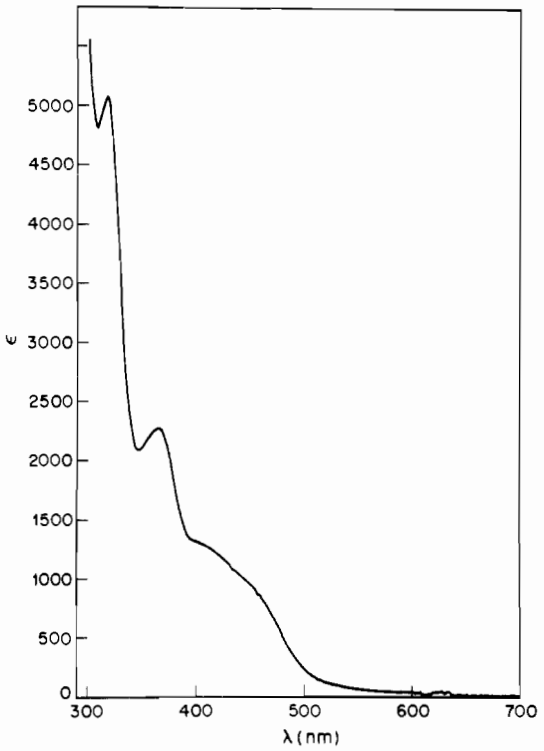

Figure 8. Electronic spectrum of $[Ir(Se_4)(dmpe)_2]Cl$ in an EPA glass at liquid-nitrogen temperature.

calculated for the Se2–Se2 bond in the Se_4 group in $[Ir(Se_4)(PH_3)_4]^+$; this compares with a bond order of 1.00 for Se_2 in $[Ir(Se_2)(PH_3)_4]^+$. The total valence charge density maps in Figure 6 support the conclusion that the Se2–Se2 covalent interaction in $[Ir(Se_4)(PH_3)_4]^+$ is slightly greater than the interaction in $[Ir(Se_2)(PH_3)_4]^+$ (cf. parts a and c of Figure 6 with part f and with Figure 8d of ref 14). Se1–Se2 covalent interaction in the Se_4 group is also mostly pσ bonding together with some uncanceled π interaction. In this case the interactions occur mainly in levels 10b and 13b and are shown in Figure 7c,d. The total valence charge density maps in Figure 6 indicate that Se1–Se2 covalent bonding in weaker than Se2–Se2 bonding (cf. Figure 6a,c,d). This is consistent with the observed bond length alternation in the chelating Se_4 group.

A possible explanation for the fact that, in contrast to the results with $[Ir(dppe)_2]Cl$ and $[Rh(dmpe)_2]Cl$, the reaction of $[Ir(dmpe)_2]Cl$ with Se_8 leads mainly to the Se_4 rather than the Se_2 complex may reside in the effect of phosphine ligand basicity on the Se_2 complex $6b_1$ orbital. We have already pointed out[14] that increasing the basicity of the phosphine ligand by changing from dppe to dmpe enhances the π M–Se_2 bonding in level $6b_1$ and that this effect is greater for the iridium than for the rhodium complex. Accompanying the increase in π M–Se_2 interaction is an increase in level $6b_1$ π^* Se–Se interaction. We suggest that the weaker Se–Se bonding in $[Ir(Se_2)(dmpe)_2]^+$ may be the cause for this complex being formed to only a minor extent in the synthesis from Se_8.

Electronic Spectrum of $[Ir(Se_4)(dmpe)_2]^+$. Figure 8 shows the electronic absorption spectrum of $[Ir(Se_4)(dmpe)_2]^+$ in the 300–700-nm region. Table IX gives the band assignments and the calculated energies for the transitions as obtained by spin-restricted transition-state calculations on $[Ir(Se_4)(PH_3)_4]^+$. The agreement between observed and calculated energies is good. All of the transitions are predominantly intra Se_4 ligand in character, although 17a → 16b, 15b → 16b, and 16a → 16b have an appreciable ligand → metal charge-transfer component. The HOMO → LUMO transition, 17a → 16b, corresponds to the shoulder at ~450 nm, which is the lowest energy feature of the spectrum. The single largest component of the HOMO → LUMO transition may be described as π^*_{xy} → pσ^* and is analogous to the largest component ($\pi^*_{\perp}$ → pσ^*) of the HOMO → LUMO transition in $[Ir(Se_2)(PH_3)_4]^+$. The major differences between the spectra of $[Ir(Se_4)(PH_3)_4]^+$ and $[Ir(Se_2)(PH_3)_4]^+$ are as follows: (1) The HOMO → LUMO transition in the Se_2 complex is shifted to lower energy (2.54 eV (observed 2.10 eV) for the Se_2 complex compared to 2.86 eV (observed ~2.76 eV) for the Se_4 complex). (2) An intense metal → ligand charge transfer occurs at 3.93 eV (observed 4.01 eV) in the Se_2 complex. The corresponding transition in the Se_4 complex, 15a → 16b, is about 0.5 eV higher in energy and is outside the range studied. Aside from the ligand to metal charge transfer, the other bands in the 300–700-nm spectrum of the Se_2 complex are predominantly intra Se_2 ligand in character, analogous to the intra Se_4 ligand character of the bands in the spectrum of the Se_4 complex.

Registry No. $[Ir(dmpe)_2]Cl$, 60314-45-6; $[Ir(Se_2)(dmpe)_2]Cl$, 85479-84-1; $[Ir(Se_4)(dmpe)_2]Cl$, 85479-85-2; $[Ir(Se_4)(PH_3)_4]^+$, 85479-86-3; Se_8, 12597-33-0; PPh_3, 603-35-0.

Supplementary Material Available: Tables of observed and calculated structure factors and thermal parameters (20 pages). Ordering information is given on any current masthead page.